Atmospheric Research 94 (2009) 254–269

Contents lists available at ScienceDirect

Atmospheric Research

journal homepage: www.elsevier.com/locate/atmos

Impact of terrain heterogeneity on near-surface turbulence structure

Clément Fesquet [a], Philippe Drobinski [a,*], Christian Barthlott [a,b], Thomas Dubos [a]

[a] Institut Pierre Simon Laplace/Laboratoire de Météorologie Dynamique, École Polytechnique/ENS/UPMC/CNRS, Palaiseau, France
[b] Universität Karlsruhe/Forschungszentrum Karlsruhe, Karlsruhe, Germany

ARTICLE INFO

Article history:
Received 27 November 2008
Received in revised form 26 May 2009
Accepted 5 June 2009

Keywords:
Atmospheric surface layer
Surface heterogeneity
Turbulence measurements
Coherent structures

ABSTRACT

This study investigates the impact of terrain heterogeneity on local turbulence measurements using 18 months of turbulence data taken on a 30 m tower at the SIRTA mixed land-use observatory under varying stability conditions and fetch configurations. These measurements show that turbulence variables such as the turbulent kinetic energy or momentum fluxes are strongly dependent on the upstream complexity of the terrain (presence of trees or buildings, open field). However, using a detection technique based on wavelet transforms which permits the isolation of the large-scale coherent structures from small-scale background fluctuations, the study shows that, for all stability conditions, whatever the upstream complexity of the terrain, the coherent structures display universal properties which are independent of the terrain nature: the frequency of occurrence, time duration of the coherent structures, the time separation between coherent structures and the relative contribution of the coherent structures to the total fluxes (momentum and heat) appear to be independent of the upstream roughness. This is an important result since coherent structures are known to transport a large portion of the total energy. This study extends to all stability conditions a numerical study by Fesquet et al. [Fesquet, C., Dupont, S., Drobinski, P., Barthlott, C., Dubos, T., 2008. Impact of terrain heterogeneities on coherent structures properties: experimental and numerical approaches. In: 18th Symposium on Boundary Layers and Turbulence. No. 11B.1. Stockholm, Sweden., Fesquet, C., Dupont, S., Drobinski, P., Dubos, T., Barthlott, C., in press. Impact of terrain heterogeneity on coherent structure properties: numerical approach. Bound.-Layer Meteorol.] conducted in neutral conditions which shows that a reason for such behavior is that the production of local active turbulence in an internal boundary layer associated with coherent structure originating from the outer layer and impinging onto the ground is not sensitive to the nature of the terrain.

1. Introduction

Turbulent exchange of momentum, heat and moisture between the atmosphere and a flat, horizontally homogeneous surface is well described by Monin–Obukhov (MO) similarity theory (Monin and Obukhov, 1954). In the framework of this theory, the scaling variables are the friction velocity, the measurement height, the Obukhov length and the roughness length. Dimensionless flux profile relationships have been estimated through careful field experiments under ideal conditions over flat sites with uniform vegetation (Businger et al., 1971; Dyer, 1974).

However, the surface of the Earth is covered with roughness elements, such as crops, forests, and urban areas, that form a patchwork mosaic of varying surface roughness. This wide range of complex surfaces disturbs the turbulent flow over the surface and influences the processes that govern the exchange of momentum, heat, and mass between the "complex" surface and the planetary boundary layer (PBL). Therefore, the surface–atmosphere interaction and the nature of the flow upstream and downstream of the obstacles themselves are only partly understood. Indeed, the surface layer has to continually adjust to the surface changes. In addition to the pressure gradients induced by the interaction

* Corresponding author.
E-mail address: philippe.drobinski@lmd.polytechnique.fr (P. Drobinski).

0169-8095/$ – see front matter © 2009 Elsevier B.V. All rights reserved.
doi:10.1016/j.atmosres.2009.06.003

of the flow with obstacles which involve a rapid response, the adjustment of the surface layer to the new surface properties by turbulent mixing is not instantaneous, but rather a gradual upward and downwind propagation through an internal boundary layer. The surface layer in this state is not spatially homogeneous nor are fluxes constant with height. As a result, similarity theory is in principle not applicable and modelers have difficulties to correctly describe the complex surface interaction.

Experimental and numerical investigations have been carried out in order to improve our understanding of turbulence dynamics in "weakly" heterogeneous terrain (Bradley, 1968; Claussen, 1987) focusing on the impact of roughness change and/or heat flux transition on turbulence properties or model parametrization (e.g. Taylor, 1968; Mahrt, 1996). These different studies suggest that close to the new surface, within the internal boundary layer, an inner "equilibrium layer" is formed. This layer is in complete adjustment to the new surface, fluxes are thus representative of the new surface and approximately constant with height, allowing similarity theory to be applied (Garratt, 1990). Moreover, recent studies by Patton et al. (2005) or Courault et al. (2007) have highlighted the disrupting effect of breeze-like circulations induced by the surface heterogeneity on the PBL structure and its energetics (turbulence fluxes and variances). The level of complexity increases when dealing with turbulence within and above a canopy. For urban canopy, Kastner–Klein and Rotach (2004) and Lien and Yee (2004) studied the mean and turbulent flow structure using a wind tunnel and numerical simulations, respectively, whereas Karlsson (1986) evaluated the applicability of different wind profile formulas using field experiment. For vegetated canopy, Baldocchi and Hutchinson (1987), Baldocchi and Meyers (1988), Marcolla et al. (2003), and Kruijt et al. (2000) studied the vertical profiles of mean and turbulence parameters within and above the vegetation using sonic anemometers data whereas Raupach et al. (1986), Seginer et al. (1976), Al-Jiboori et al. (2001), and Villani (2003) investigated in complement the vertical profiles of turbulent velocity spectra using wind-tunnel and field experiments. Flow structure upstream and downstream of high topographical elements such as a forest edge has been analyzed for instance by Raynor (1971) and Gash (1986). The case of forests is particularly complex since forests represent, aerodynamically, a change in roughness, porosity and effective surface height (zero plane displacement). Morse et al. (2002) and Irvine et al. (1997) studied the turbulent airflow development downwind of a forest transition by presenting point measurements across a smooth to rough transition. Liu et al. (1996) made E–ε simulations of the turbulence pattern downwind a forest edge. It should be also noted that consecutive arrangement of obstacles can significantly modify the flow and turbulence properties (i.e. in wake interference flow and skimming flow), horizontally homogeneous conditions can be restored with an inertial sublayer above (e.g. observed in cities or forests).

In a turbulent air flow, turbulence is generally composed of both disorganized motion and more organized motion, also called coherent structures which can take the form of convective PBL rolls or cells (e.g. Etling and Brown, 1993; Drobinski et al., 1998), near-surface streaks (e.g. Drobinski and Foster, 2003; Drobinski et al., 2004, 2007) and waves (e.g. Mahrt, 1999), depending on the atmospheric stability. According to Barthlott et al. (2007), the contribution of the coherent structures to the overall transport is most often about 50% with a broad probability distribution (from 30 to 70%) consistent with other published results: 75% (Gao et al., 1989), 40% (Lu and Fitzjarrald, 1994), 60% (Drobinski et al., 2004) and about 30% (Feigenwinter and Vogt, 2005). Only few numerical simulations and nearly no experimental studies address the questions of the dynamics of the coherent structures in the context of a "complex" terrain and the modulation of the coherent structure contribution to the turbulence fluxes by the complex elements of the terrain. This is a fundamental issue since it has been shown that the contribution of coherent structures on the turbulent fluxes needs to be accounted for in subgrid-scale parameterizations of meso-scale to global-scale models (e.g. Foster and Brown, 1994; Morrison et al., 2005; Drobinski et al., 2006).

In a previous study (Fesquet et al., 2008, in press), the impact of surface heterogeneity on near-surface turbulence structure was investigated experimentally and numerically in a neutral PBL. Using the same detection technique as Barthlott et al. (2007), based on wavelet transforms, which permits the isolation of the large-scale coherent structures from small-scale background fluctuations, the numerical study, based on large-eddy simulation (LES), showed that whatever the upstream complexity of the terrain (forest or open field), coherent structures display universal properties such as the frequency of occurrence, duration and separation times and relative contribution to total fluxes (momentum and heat). This numerical investigation also showed that the region of development of structures is located well above surface heterogeneities, in the outer layer, where shear instabilities induce structures that are hereafter transported downward onto the ground through a 'top–down' mechanism. The production of local active turbulence in the internal boundary layer associated with the impinging coherent structure is independent to the surface nature.

The present paper can be seen as an extension of Fesquet et al. (2008) and Fesquet et al. (in press) study to all stability conditions, i.e. from very stable to very unstable stratification. We take advantage of the long-term database of high-frequency measurements collected by sonic anemometers at 10 and 30 m heights at the SIRTA observatory located at Palaiseau, 20 km south of Paris, France (Haeffelin et al., 2005). The observatory is located on a plateau in a semi-urban environment divided equally in agricultural fields, wooded areas, and sparse housing and industrial developments. The data set covers all types of meteorological situations and stratification and allows the identification of coherent structures and the derivation of their structural and energetic properties. Using this data set, we address the following questions:

- What is the impact of terrain heterogeneities on the average turbulence variables such as turbulent kinetic energy and momentum and heat fluxes for different stability conditions?
- What is the impact of terrain complexity on the coherent structure properties such as their frequency of occurrence (number of structures detected in 30-min period), their duration and separation times and their relative contribution to the turbulent fluxes, in very stable to very unstable PBLs?

After the introduction in Section 1, Section 2 describes the main characteristics of the SIRTA observatory, Section 3 shows

the impact of the upstream topographical elements to the average turbulence variables (momentum and heat fluxes, turbulent kinetic energy). Section 4 recalls the methodology of coherent structure extraction and discusses the coherent structure properties as a function of upstream complexity of the terrain, and stratification. Finally, Section 5 concludes the study and suggests still open questions to be addressed in future work.

2. Characteristics of the research site

2.1. Research site

Since April 2005, turbulence data have been collected at the French ground-based remote sensing atmospheric observatory, SIRTA (Haeffelin et al., 2005), located in a mixed land-use environment, in Palaiseau, 20 km south of Paris. SIRTA operates a 30 m mast instrumented with two sonic anemometers at 10 and 30 m heights. The observatory sits on a 10-km plateau about 160 m above sea level. The plateau is a semi-urban environment divided equally in agricultural fields, wooded areas, and sparse housing and industrial developments. In Drobinski et al. (2006) and Barthlott et al. (2007), only the prevailing westerly winds are considered since this sector corresponds to a homogeneous terrain grass field upstream of the mast, so the two measurement levels are in the atmospheric surface layer (ASL) above the roughness sublayer (which is approximately 30 cm deep). In this study, the other wind sectors are analyzed since complex topographical elements are located upstream of the mast (Fig. 1).

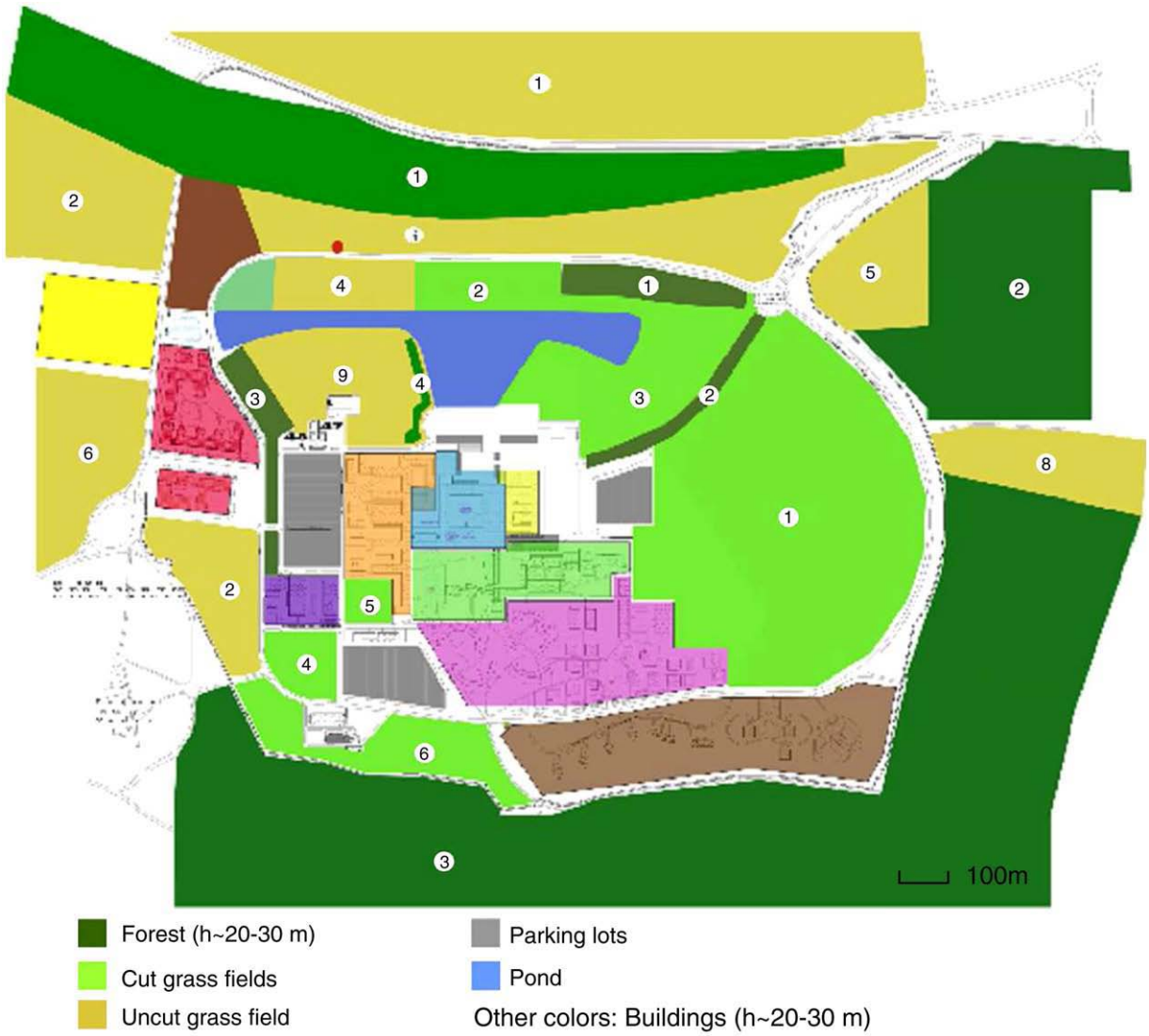

Fig. 1. Map of the École Polytechnique campus hosting the SIRTA observatory. The colors correspond to various typical terrain types. The red dot located in the uncut grass field indicates the location of the 30 m measurement tower. (For interpretation of the references to color in this figure legend, the reader is referred to the web version of this article.)

Indeed, north of the mast, at about 70 m, there is a forest barrier about 50 m width (i.e. $x/h \sim 3$–4 where x is the fetch distance and $h \sim 20$ m, the height of the topographical element). East of the mast, there is a distant forest, at about 400 m (i.e. $x/h \sim 15$–20). In the south direction, there are the laboratory buildings at about 300 m (i.e. $x/h \sim 10$–15). West of the mast, there is an open field, thus chosen as the reference direction.

The two sonic anemometers record the data at 10 Hz sampling frequency. Many studies were conducted on sonic anemometer data processing in order to give access to the mean meteorological variables (wind speed and direction and temperature which is approximately equal to virtual temperature) and to the second-order moment statistics of these variables (variances and fluxes): Champagne et al. (1977) used averages on about 1-min whereas McAneny et al. (1988) averaged over 5-min (3000 samples) and Drobinski et al. (1998) and Peters et al. (1998) over 10-min (6000 samples). Most published articles use averaging periods between 5 and 10-min. Vickers and Mahrt (1997) chose to average their data over a 5 min period, for a best compromise between sampling error and representativeness due to shift in wind direction. We conducted a sensitivity study using 5-min and 30-min averaging periods. No differences were found on the turbulent variable values but the scatter was reduced using the 30-min averaging period. Since a 30-min averaging period is used for coherent structure detection (see Section 4 and Barthlott et al., 2007), we thus use for consistency a 30-min averaging period for all data processing. The data set used in this study corresponds to the period extending between April 2005 and October 2006, covering all types of meteorological situations and stratification (from stable to convective). Both the 10-Hz and 30-min averaged data are stored and processed in this study.

2.2. Data processing

In order to have u' as the streamwise velocity fluctuations, we first rotate the coordinate system with the downstream direction x' along and the crossstream direction y' perpendicular to the mean flow, so that $u' = u\cos\alpha + v\sin\alpha$ and $v' = -u\sin\alpha + v\cos\alpha$, with u and v the turbulent horizontal velocity components and α the wind direction. Following Deardorff (1972), local stratification in the PBL can be expressed by z_i/L_*, where z_i is the PBL inversion height and L_* is the Obukhov length given by:

$$L_* = -\frac{u_*^3\,\overline{T}}{kg\,\overline{w'T'}} \tag{1}$$

where T is the temperature, k the Von Karman constant ($k \approx 0.4$), g the gravity acceleration, w' the vertical velocity fluctuations, T' the temperature fluctuations and u_* the friction velocity defined by:

$$u_* = \left(\overline{u'w'}^2 + \overline{v'w'}^2\right)^{1/4}, \tag{2}$$

with u', v', the deviations of the horizontal velocity components calculated from the 30-min averaged mean values. The average mean ($\overline{T}$) and turbulence variables ($\overline{u'w'}$, $\overline{v'w'}$ and $\overline{w'T'}$) are directly computed from the sonic anemometer measurements; $z_i/L_* < 0$ (>0) indicates thermal instability

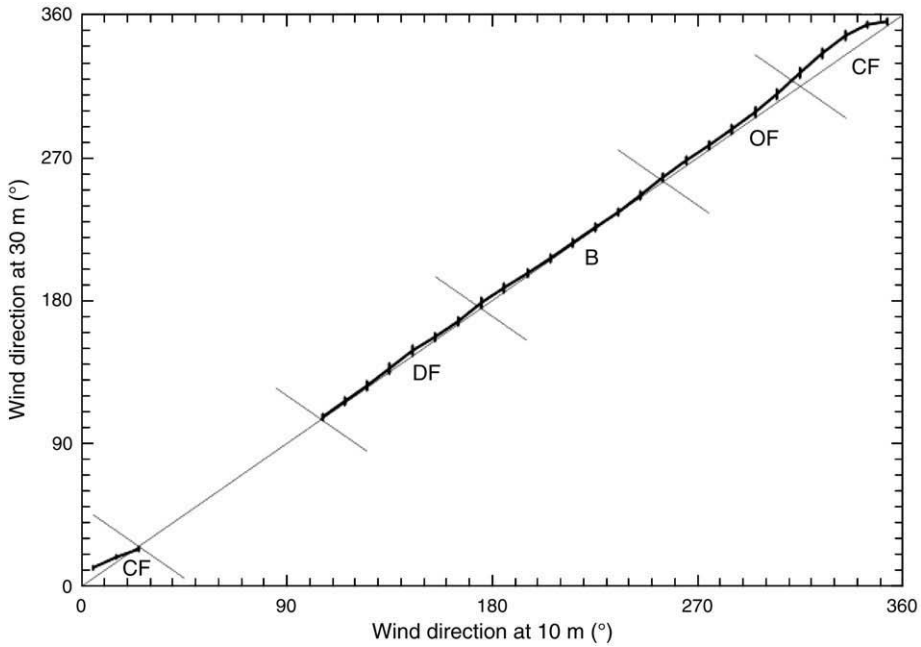

Fig. 2. Wind direction measured at 30 m height versus wind direction measured at 10 m height. Notations CF, DF, B and OF correspond to the close forest, distant forest, buildings and open field wind sectors, respectively.

Table 1
Available reliable data (h) for the different stability regimes after quality control as a function of wind direction.

	Very stable	Stable	Unstable	Very unstable	Total
Close forest					
10 m data (h)	81.5	105.5	220.5	249	656.5
30 m data (h)	816	336.5	352.5	443	1948
Distant forest					
10 m data (h)	328.5	65	50.5	343.5	787.5
30 m data (h)	346	190	96.5	243.5	876
Buildings					
10 m data (h)	378	466	314	566.5	1724.5
30 m data (h)	287	382.5	413.5	282.5	1365.5
Open field					
10 m data (h)	741	219	206.5	818.5	1985
30 m data (h)	737	307.5	315	600	1959.5

(stability). The surface momentum and heat fluxes are equal to ρu_*^2 and $\rho C_p u_* T_*$ respectively, where ρ is the air density, C_p the specific heat at constant pressure, and T_* the scaling temperature given by:

$$T_* = -\frac{\overline{w'T'}}{u_*} \quad (3)$$

The data set between April 2005 and October 2006 represents approximately 215 days (256 days) of data available at 10 m (at 30 m) after quality control (see details in Barthlott et al., 2007).

2.3. Classification according to upstream terrain

The data set is clustered as a function of wind direction. A comparison between the wind direction measured at 10 and 30 m heights is shown in Fig. 2. We define four different wind direction sectors:

1. The wind sector ranging between 310° and 30° corresponds to a close forest about 70 m upstream of the measurement tower to the north. The forest height is about 20 m so $x/h \sim 3$–4. In this situation, the wind at 30 m is slightly shifted to the east with respect to that at 10 m (Fig. 2) since the low level flow turns around the vegetation belt so the flow measured at 10 m is more disturbed than the flow measured at the 30 m measurement point (Nord, 1991).
2. The wind sector ranging between 100° and 170° corresponds to a distant forest which is about 400 m upstream of the measurement tower to the east (i.e. $x/h \sim 15$–20). Fig. 2 shows a perfect match between wind direction at 10 and 30 m heights as would be the case over perfectly flat terrain. Indeed, the wind veering decreases with increasing distance to the forest edge.
3. The wind sector ranging between 170° and 260° corresponds to a group of buildings located 300 m to the south of the measurement tower (i.e. $x/h \sim 10$–15).
4. The wind sector ranging between 260° and 310° corresponds to an open field sector to the west. The terrain "seen" by the instrumented tower is fairly flat and homogeneous, the turbulent fluxes as well as the wind direction are constant with height (Drobinski et al., 2006).

It must be noticed that the measurement tower is located over a grass field with at least 70 m fetch (distance from terrain property change) in all directions. We did not use the data in the 30°–100° sector because when the wind blows from this sector, the anemometers are in the tower wake and the data are no longer reliable (Barthlott and Fiedler, 2003). Finally, after quality control, the number of hours of observations per wind sector and stability conditions is given in Table 1; Fig. 3 shows the probability distribution function of the wind direction at 10 m with a peak about

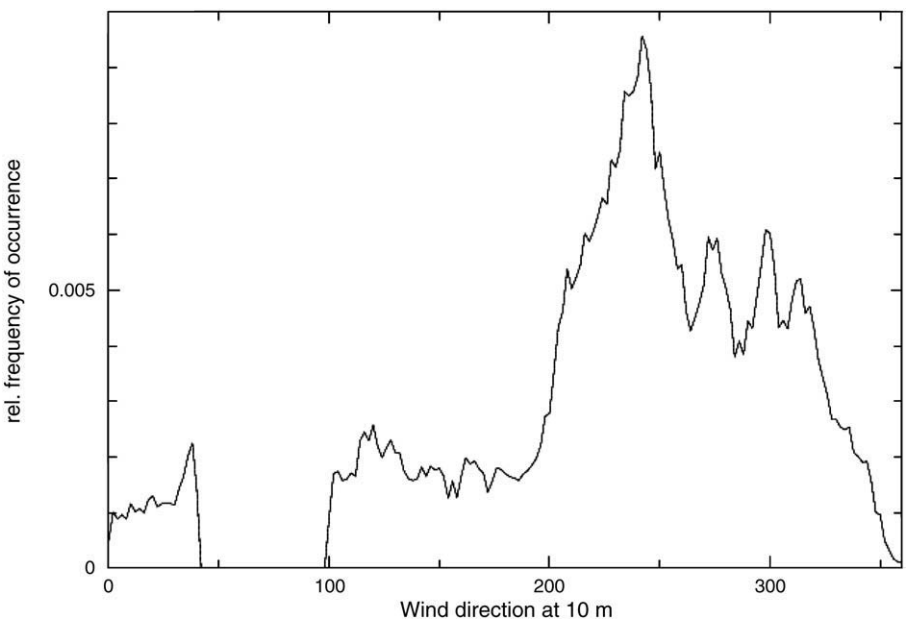

Fig. 3. Probability distribution function of the wind direction at 10 m.

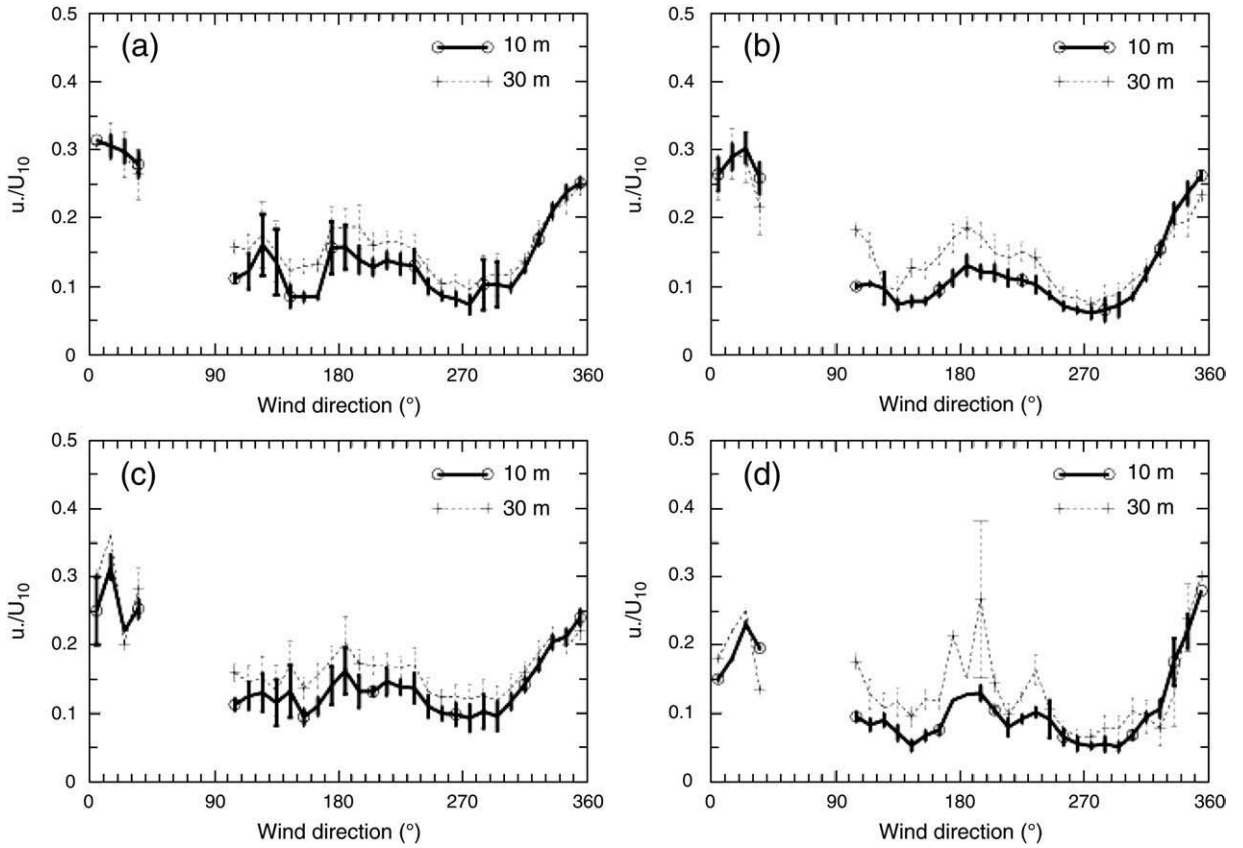

Fig. 4. Normalised friction velocity u_*/U_{10} at 10 m (solid line) and 30 m (dashed line) as a function of the 10-m wind direction and stratification. Panels a, b, c and d correspond to the unstable, stable, very unstable and very stable situations, respectively. The bars indicate the $1-\sigma$ uncertainty.

240° (direction south west–west). The stability regimes are classified as a function of the Obukhov length (L_*): the very unstable regime corresponds to $-200<L_*<0$, the unstable regime to $-1000<L_*\leq-200$, the stable regime to $200\leq L_*<1000$ and the very stable regime to $0\leq L_*<200$ (as used in Barthlott et al., 2007).

3. Near-surface turbulent kinetic energy momentum and sensible heat fluxes

When describing the turbulent flow structure in the surface layer, many authors use the friction velocity (u_*), the scaling temperature (T_*) and the turbulent kinetic energy (e) as scaling parameters. u_* and T_* are derived from the momentum and sensible heat flux, respectively, whereas $e=(1/2)(\overline{u'^2}+\overline{v'^2}+\overline{w'^2})$ characterizes the turbulence intensity per unit mass. Figs. 4, 5 and 6 show values of the normalized friction velocity u_*/U_{10} , where U_{10} is the mean streamwise velocity at 10 m, T_* and the normalized turbulent kinetic energy e/u_*^2, averaged on 10° sectors with the standard deviations associated ($1-\sigma$ uncertainty), as function of the wind direction and stability. In stably and neutrally stratified PBL over flat terrain, the momentum and heat fluxes (and so u_* and T_*) are homogeneous in the atmospheric surface layer whereas they are expected to slightly decrease with height (by less that 10%) in the convective PBL (see Stull, 1988).

Fig. 4 illustrates the effect of upstream terrain complexity on the friction velocity u_*. Indeed, the 30-min u_*/U_{10} measured at 10 and 30 m depend on the wind speed and stratification and varies as a function of the 30-min mean wind direction: the lower values of u_*/U_{10} are found for the open field sector (west) whereas it increases with increasing upstream roughness, the maximum u_*/U_{10} values being downstream of the buildings (south). One can also notice, particularly for very stably and stably stratified PBL, a significant difference (i.e. larger than one standard deviation) between the measurements at 10 and 30 m with larger u_*/U_{10} values at 30 m particularly for wind sectors corresponding to upstream distant forest and buildings. The reason for such behavior has been extensively studied: the airflow is disrupted as it flows across the roughness elements. The distortion of the flow generates strong local shear which generates turbulence. The wind then advects enhanced turbulence downstream of the roughness elements towards the 30 m mast. In the presence of the forest or the building, local advection and pressure gradient can thus no longer be neglected in the Reynolds averaged equation of motion, so the turbulent flux divergence is not zero and the turbulent fluxes vary with height. Downwind from a surface roughness change, several authors (Raine and Stevenson, 1977; Liu et al.,

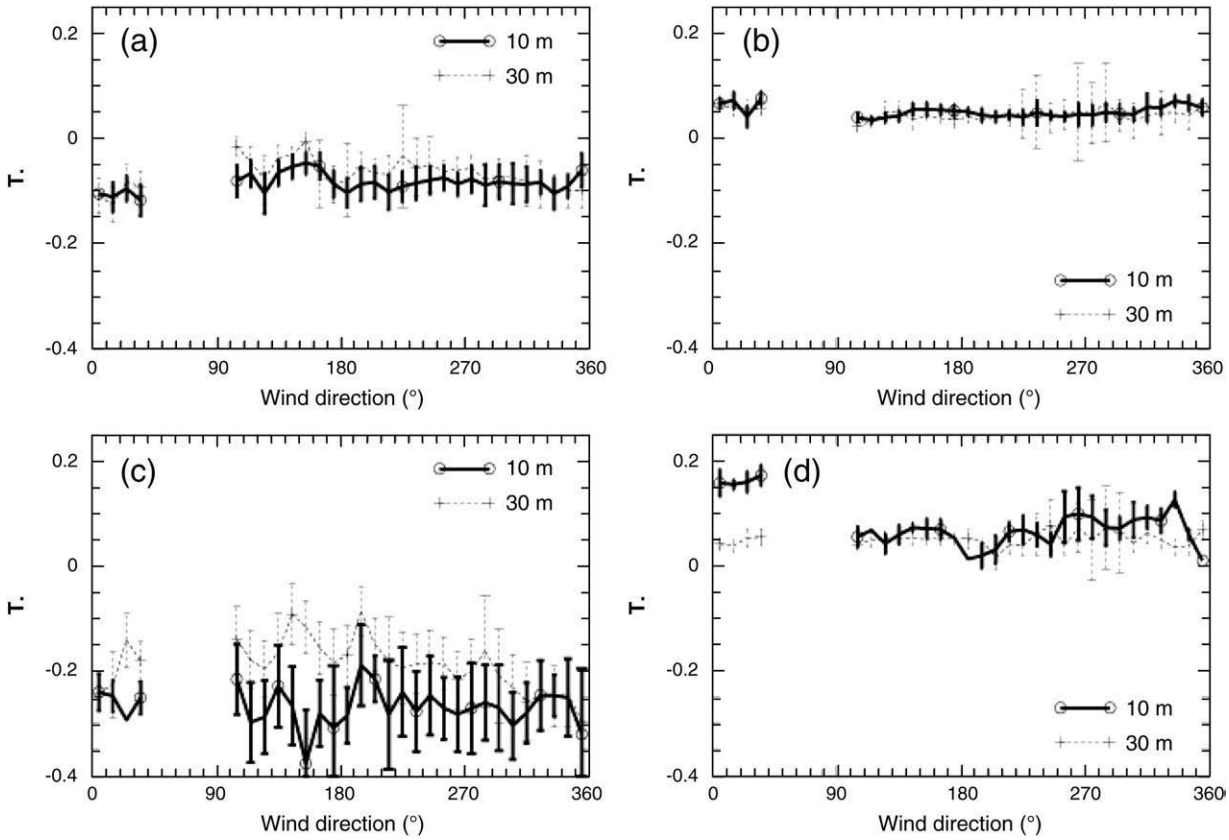

Fig. 5. Same as Fig. 4 but for T_*.

1996) used to distinguish 3 different regions in the turbulent flow: the quiet zone ($0<x/h<3.5$), the wake zone ($3.5<x/h<18$) and the readjustment zone ($x/h>18$). For our most homogeneous sectors (open field, west sector), the values of u_*/U_{10} and T_* measured at 10 and 30 m are very similar (within one standard deviation), contrary to the sector associated with the distant forest and the buildings, located between the wake and readjustment zones (easterly and southerly winds, respectively), for which the values of u_*/U_{10} measured at 30 m are significantly larger than those measured at 10 m. For the north sector (tree fence upstream of the tower and $x/h \sim 3$–4), the two anemometers are located within the wake zone where strong shear-induced mixing occurs, homogenizing the vertical profile of u_*/U_{10} at the two levels. The observed values of the friction velocity u_*/U_{10} are also strongly dependent on stratification. For very unstable conditions, the differences are minimum between 10 and 30 m heights and wind sectors (i.e. within the uncertainty bars). This is consistent with the fact that, in this stability class, the source of turbulence is local and essentially of thermal origin, and one can notice the weak dependence of u_*/U_{10} on the wind direction. This difference between 10 and 30 m becomes significant for unstable (i.e. shear-driven convective PBL), stable and very stable conditions. Under such conditions, the main source of turbulence is shear (maximum due to the topographical elements) and advection is dominant favoring turbulence transport to the measurement tower.

The situation is somehow different for T_* (Fig. 5). Indeed, surface heat fluxes are very small for stable and neutral conditions at the SIRTA observatory so the distinction between the different wind sectors is completely masked by the intrinsic uncertainty. In very unstable conditions, the footprint is very small and the forcing is mostly of thermal origin and thus local so the upstream heterogeneity is not felt at the tower. Indeed, the values of T_* are fairly homogeneous with respect to the wind direction (less than 20% variability) with, however, one peak at about 160° which corresponds to upstream buildings. The still present signature of the upstream buildings on the measured turbulence variables for the "very unstable" stability class may be due to the fact that even for weakly shear-driven convective PBL, the impact of advection may not be negligible (however, decreasing the number of data in this stability class may affect the reliability of the statistics). Finally, we can see slightly weaker values of T_* (in absolute value) at 30 m than at 10 m by 20% maximum (about 10% on average) but the uncertainty bars are large.

The normalized turbulent kinetic energy e/u_*^2 displays similar features: e/u_*^2 is strongly affected by upstream roughness in very stable, stable and unstable conditions with large differences between 10 and 30 m heights, whereas more or less homogeneous e/u_*^2 values are expected as a function of height for these stability regimes (Stull, 1988).

The largest difference is found for the east and south wind sectors whereas nearly no difference is found for the north

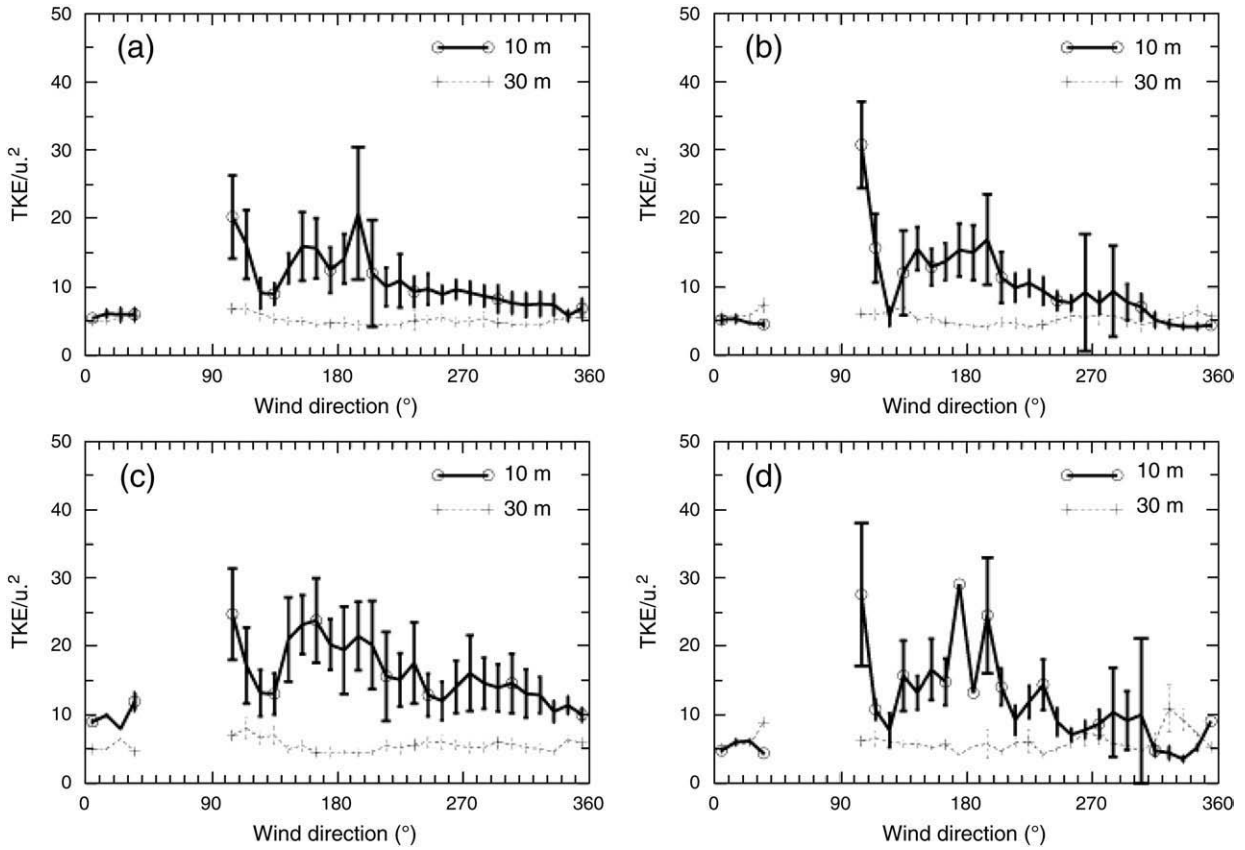

Fig. 6. Same as Fig. 4 but for the normalized turbulent kinetic energy e/u_*^2. The value of e/u_*^2 at 10 m (30 m) corresponds to the ratio between e and u_*^2 measured at 10 m (30 m).

and west sectors (close forest and open field, respectively). Shear-induced turbulent kinetic energy production is very strong at 10 m height and very dependent on the wind sectors whereas at 30 m, shear-production is weaker (less shear) and rapidly balanced by dissipation thus generating weaker turbulent kinetic energy and lower dependence on the wind sector. For northerly winds, the tower being in the wake zone of the tree fence, strong vertical mixing and homogeneous e/u_*^2 values are measured between 10 and 30 m as suggested numerically by Liu et al. (1996). For very unstable conditions, the dependence of e/u_*^2 on the 313 wind direction becomes very weak, as expected, except for the wind sector corresponding to the buildings upstream of the tower (see above).

4. Coherent structures

Atmospheric turbulence is generally composed of both disorganized motion and more organized motion. Depending on the PBL stratification, the coherent structures can take the form of convective cells (very unstably stratified PBL) or longitudinal rolls (sheared unstably stratified PBL) (e.g. Drobinski et al., 1998), streaks (shear-driven PBL) (e.g. Drobinski and Foster, 2003; Drobinski et al., 2004, 2007) and waves (stably stratified PBL) (e.g. Mahrt, 1999).

In this study, the identification of coherent structures consists in detecting ramp-like patterns in the time series of the temperature fluctuations using a wavelet analysis (see details in Barthlott et al., 2007). This analysis involves a wavelet transform which is well suited to the detection of non-periodic signals with variable durations. The one-dimensional continuous wavelet transform of a function $x(t)$ with respect to an analyzing wavelet $\psi(t)$ is defined as:

$$W_n(s) = \frac{1}{s}\int_{-\infty}^{\infty} x(t)\psi\left(\frac{t-n}{s}\right)dt \quad (4)$$

where s is a scale dilation and n a position translation. A wavelet ψ is a real or complex valued function that must have zero mean. By varying the wavelet scale s and translating along the localized time index n, one can construct a picture showing both the amplitude of any patterns and how this amplitude varies with time (Torrence and Compo, 1998). The choice of the wavelet is of particular importance, since the resulting correlation pattern will reflect the characteristics of the wavelet. The wavelet should possess a good localization in frequency space for the determination of characteristic scale, but should also be well localized in time space for event detection. Collineau and Brunet (1993a) demonstrated the advantages of the Mexican–Hat wavelet for jump detection. The Mexican–Hat wavelet is a compromise between a good frequency localization and a sufficient localization in time space. In addition, this wavelet reacts to the second derivative

of the signal, which has a change in sign (a zero-crossing) at discontinuities such as ramps. Hence this method avoids the uncertainty of empirically setting optimum detection thresholds, which is required for other wavelets (e.g., Haar, Ramp, Morlet). A number of authors have therefore used the Mexican–Hat wavelet and the zero-crossing of the wavelet coefficients to detect coherent structures in temperature time series (Chen et al., 1997; Brunet and Irvine, 2000; Feigenwinter and Vogt, 2005). In order to establish the most representative scale of the coherent structures, the global wavelet spectrum $\overline{W}(s)$ is computed as follows:

$$\overline{W}(s) = \int_{-\infty}^{\infty} |W_n(s)|^2 dn \quad (5)$$

According to Collineau and Brunet (1993a), the time scale associated with the maximum of $\overline{W}(s)$ corresponds to the mean duration of the most energetic turbulent structures.

Despite the efforts of investigating coherent structures, in recent years, the definition of these boundaries are still not established (Krusche and De Oliveira, 2004). Some authors such as Collineau and Brunet (1993b); Lu and Fitzjarrald (1994); Qiu et al. (1995); Feigenwinter and Vogt (2005) included in their definition of the coherent structures, portions of temperature fluctuation time series that follow the sudden fall (i.e. microfront). Following the approach of Antonia et al. (1979), the microfront determines the temporal/spatial end of the structure for convective conditions whereas it determines its beginning in case of stable stratification where the pattern is inverted. Hence, under convective conditions, the end of the structure is represented by zero-crossings from positive to negative values whereas the beginning of the structure is represented from negative to positive values for the case of stable stratification. The different slope sign for stable and unstable conditions is due to different characteristics of the temperature ramps (unstable: gradual rise followed by sudden fall; stable: sudden rise followed by gradual fall). In order to derive parameters like duration, separation or contribution to the turbulent transport, the other boundary of the structure has to be specified. Some authors use a fixed time window around the zero-crossing of the wavelet coefficients (Feigenwinter and Vogt, 2005) or the nearest zero-crossings in both directions of the microfront (Qiu et al., 1995).

Gao et al. (1989) determines the length of a structure by taking into account the region with continuous updrafts preceeding the microfront to the region with continuous downdraft afterwards. The determination of the mean duration by the maximum of the global wavelet spectrum (applied by Gao and Li, 1993; Lu and Fitzjarrald, 1994) can be influenced by the fact that the ramp patterns can have varying duration and separation times between ramps even inside an analyzed 30-min period (which is the block chosen for this study).

An improved approach is presented here where the graduation of the time series using the wavelet coefficients allows a dynamical adjustment to the varying scales as accurately as possible: starting from each microfront (detected by the zero-crossing of the wavelet coefficients), we use the preceeding minimum of the coefficients under convective conditions or the following one for stable situations to determine the duration D of each coherent structure separately. The remaining parts of the time series are the separation times S. Especially for the separation times, this method provides a more accurate result since long ramp-free periods and shorter separation times are detected as well. By doing this, we take into account the internal variability inside a 30-min period and have now the separation times between two detected structures which are not only calculated by the number of detections per data block. Another advantage is that the calculation of probability distributions can be based on all detected structures and not on half-hourly averaged duration or separation times.

Collineau and Brunet (1993a) pointed out that the zero crossing method using the Mexican–Hat wavelet might identify too many structures during long ramp-free periods. For this reason, we introduce a threshold value for the detection: a coherent structure is identified only by those zero-crossings of the wavelet coefficients whose corresponding maximum (representing the amplitude of the ramp) exceeds at least 40% of the total maximum of the coefficient at the analyzed scale. The introduction of this selection criterion is a necessary supplementation when regarding long-term measurements which may include ramp-free periods. Another advantage of our method is the avoidance of overlapping structures which may caused problems in the works of Lu and Fitzjarrald (1994) and Feigenwinter and Vogt (2005).

Table 2
Mean values of coherent structure frequency of occurrence (FO) and contribution to the momentum ($F_{coh}uw$) and heat ($F_{coh}wT$) fluxes, for the four stability classes and the four wind sectors at 10 and 30 m measurement points as well as their uncertainty ($\simeq \pm 10\%$ on average, computed by subdividing the data set and estimating the variability of the mean value estimates for the different sub-datasets).

	Very stable	Stable	Unstable	Very unstable
Close forest				
$F_{coh}(uw)_{10\ m}$ (%)	46 ± 6	44 ± 6	37 ± 5	42 ± 3
$F_{coh}(wT)_{10\ m}$ (%)	45 ± 6	48 ± 6	44 ± 6	45 ± 2
$FO_{10\ m}$ (30 min^{-1})	12 ± 2	11 ± 3	8 ± 1	8 ± 2
$F_{coh}(uw)_{30\ m}$ (%)	43 ± 3	39 ± 3	42 ± 5	53 ± 3
$F_{coh}(wT)_{30\ m}$ (%)	42 ± 3	42 ± 2	45 ± 3	51 ± 2
FO_{30m} (30 min^{-1})	11 ± 1	10 ± 1	8 ± 1	7 ± 1
Distant forest				
$F_{coh}(uw)_{10\ m}$ (%)	51 ± 6	42 ± 9	38 ± 20	48 ± 4
$F_{coh}(wT)_{10\ m}$ (%)	48 ± 5	31 ± 11	64 ± 13	49 ± 2
FO_{10m} (30 min^{-1})	10 ± 1	8 ± 5	9 ± 2	8 ± 1
$F_{coh}(uw)_{30\ m}$ (%)	44 ± 5	44 ± 4	42 ± 10	50 ± 6
$F_{coh}(wT)_{30\ m}$ (%)	45 ± 4	47 ± 2	55 ± 10	50 ± 4
FO_{30m} (30 min^{-1})	10 ± 1	10 ± 1	8 ± 1	6 ± 1
Buildings				
$F_{coh}(uw)_{10\ m}$ (%)	46 ± 4	39 ± 4	38 ± 3	42 ± 2
$F_{coh}(wT)_{10\ m}$ (%)	44 ± 3	42 ± 5	46 ± 3	46 ± 2
FO_{10m} (30 min^{-1})	10 ± 1	9 ± 1	8 ± 1	8 ± 1
$F_{coh}(uw)_{30\ m}$ (%)	40 ± 3	39 ± 2	40 ± 2	49 ± 3
$F_{coh}(wT)_{30\ m}$ (%)	44 ± 2	45 ± 3	46 ± 4	50 ± 2
FO_{30m} (30 min^{-1})	9 ± 1	9 ± 1	8 ± 1	7 ± 1
Open field				
$F_{coh}(uw)_{10\ m}$ (%)	46 ± 4	40 ± 6	35 ± 6	45 ± 3
$F_{coh}(wT)_{10\ m}$ (%)	46 ± 2	42 ± 5	48 ± 5	48 ± 2
FO_{10m} (30 min^{-1})	11 ± 1	10 ± 1	7 ± 2	7 ± 1
$F_{coh}(uw)_{30\ m}$ (%)	43 ± 2	39 ± 3	39 ± 4	50 ± 2
$F_{coh}(wT)_{30\ m}$ (%)	45 ± 2	44 ± 4	47 ± 6	51 ± 2
FO_{30m} (30 min^{-1})	11 ± 1	9 ± 1	7 ± 1	7 ± 1

The individual steps of our detection method for a given temperature time series are as follows:

1. remove small-scale fluctuations by digital filtering based on a fast Fourier transform (cut-off frequency 2 Hz);
2. lower the sampling frequency from 10 Hz to 1 Hz and remove a linear trend;
3. calculate wavelet transforms for 30 min data runs and the global wavelet spectrum using the Mexican–Hat wavelet, and then
4. analyze the wavelet coefficients at the peak scale of the global wavelet spectrum depending on the type of stability
   - for unstable stratification:
   - determine the ending points of the structures by each zero-crossing of the wavelet coefficients with a negative slope whose preceeding local maximum exceeds a value of 0.4 times the absolute maximum of the coefficients at that scale, and
   - determine each starting point by the preceeding minimum of the wavelet coefficients.
   - for stable stratification:
   - determine the starting points of the structures by each zero-crossing of the wavelet coefficients with a positive slope whose following local maximum exceeds a value of 0.4 times the absolute maximum of the coefficients at that scale, and
   - determine each ending point by the following minimum of the wavelet coefficients.

The results of this study are not influenced by steps 1 and 2, since they just smooth the time series and reduce the computation time. The large-scale signal remains unaltered. However, the choice of the threshold criteria has a strong impact on our results if long ramp-free periods exist. We tested a number of threshold values ranging from 20% to 60% for several days of measurements, the value of 40% seemed to be the most appropriate one.

With this value, the bulk of the occurring structures was detected, structures on smaller scales were also detected and random-like fluctuations during ramp-free periods were discarded. In the range of 40%, the number of detected structures did not vary as much as in the range around 60% or 20%. However, false detections cannot be completely excluded, which is the reason why a visual inspection of all treated data-blocks was performed after the wavelet detection algorithm. Then, our wavelet analysis of the temperature fluctuations allows the detection of sweeps or ejections associated with the presence of coherent structures at the instrumented tower, the localization of the coherent structures in time, the quantification of their life time and their occurrence and the estimation of their contribution to the turbulent transport calculated

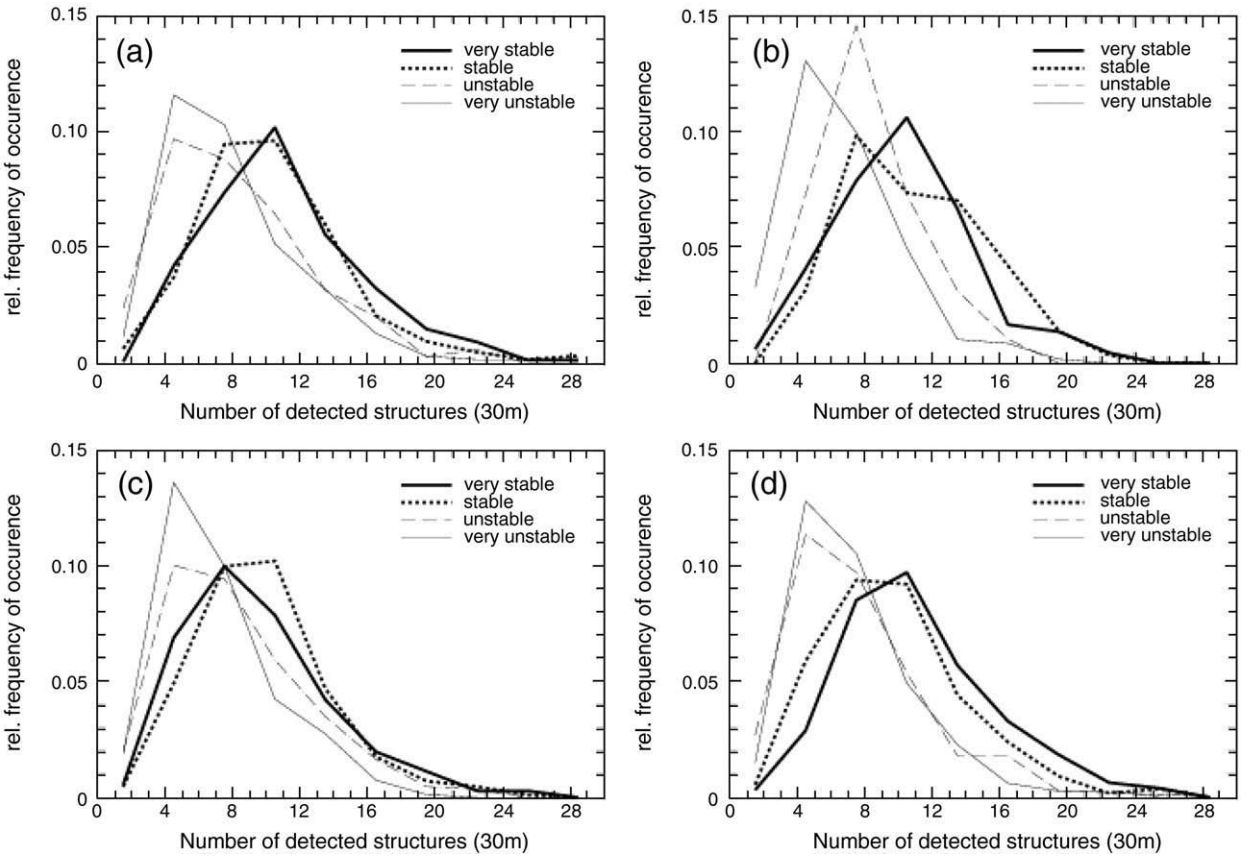

Fig. 7. Probability distribution functions of coherent structures occurrence per 30 min time period, obtained from the measurements collected at 30 m as function of stratification. Panels a, b, c and d correspond to the north (close forest), east (distant forest), south (buildings) and west (open field) sectors, respectively.

as follows (the notations are those of Barthlott et al. (2007)):

$$F_{\mathrm{coh}} = \left\{ \sum_{i=1}^{\mathrm{no}} \overline{w'x'}_{\mathrm{coh}} \times t_{\mathrm{coh}} \right\} / \left(\overline{w'x'} \times t \right) \text{ with :} \quad (6)$$

$$\overline{w'x'}_{\mathrm{coh}} = t_{\mathrm{coh}}^{-1} \sum \left(w - \overline{w} \right) \left(x - \overline{x} \right) \Big|_{\mathrm{coh}} \quad (7)$$

$$\overline{w'x'} = t^{-1} \sum \left(w - \overline{w} \right) \left(x - \overline{x} \right) \quad (8)$$

The quantities $\overline{w}$ and $\overline{x}$ are calculated over the entire half-hour period t, where x represents temperature T or the longitudinal velocity component u and no is the number of detected structures. The quantity $\overline{w'x'}_{\mathrm{coh}}$ is the conditionally averaged flux of variable x for each coherent structure with duration t_{coh} and $\overline{w'x'}$ stands for the total Reynolds averaged turbulent flux.

Table 2 summarizes the mean values of the frequency of occurrence of the coherent structure (FO) and their relative contribution to the momentum ($F_{\mathrm{coh}}(uw)$) and heat ($F_{\mathrm{coh}}(wT)$) fluxes for the four stability classes and the four wind sectors at 10 and 30 m heights; as well as their uncertainty (≃10%, computed by subdividing the data set and estimating the variability of the mean value estimates for the different sub-datasets). One striking feature is the absence of significant difference between the different sectors (within one standard deviation) whatever the stability conditions despite the strong dependence on the averaged turbulent variables such as kinetic energy and fluxes found in Section 3. This is consistent with the numerical study by Fesquet et al. (2008, in press) for neutral PBL.

This strong similarity between the wind sectors is not only seen on the mean values but also on the probability distribution functions (PDF) which is a much more demanding criterion. We display the PDF for coherent structure occurrence (Fig. 7), coherent structure contribution to momentum (Fig. 8) and sensible heat fluxes (Fig. 9) at 30 m height. Very similar results are obtained at 10 m height but are not shown. Fig. 7 displays the PDF of coherent structure occurrence on 30 min period as a function of the wind sectors and the stability. We observe on average between 6 and 12 structures every 30 min with no clear deterministic relationship between the coherent structures occurrence and the stability (in agreement with Gao et al., 1992), but more structures are detected under stable stratification than for convective conditions. Our values are comparable to other studies (e.g. Feigenwinter and Vogt (2005): 7–10 structures per 30 min). Despite some noise due to the limited number of data used to compute the PDFs for the four wind sectors and stability classes, the PDFs are very similar for all wind sectors and a given stability class. This feature is also found in Fig. 8

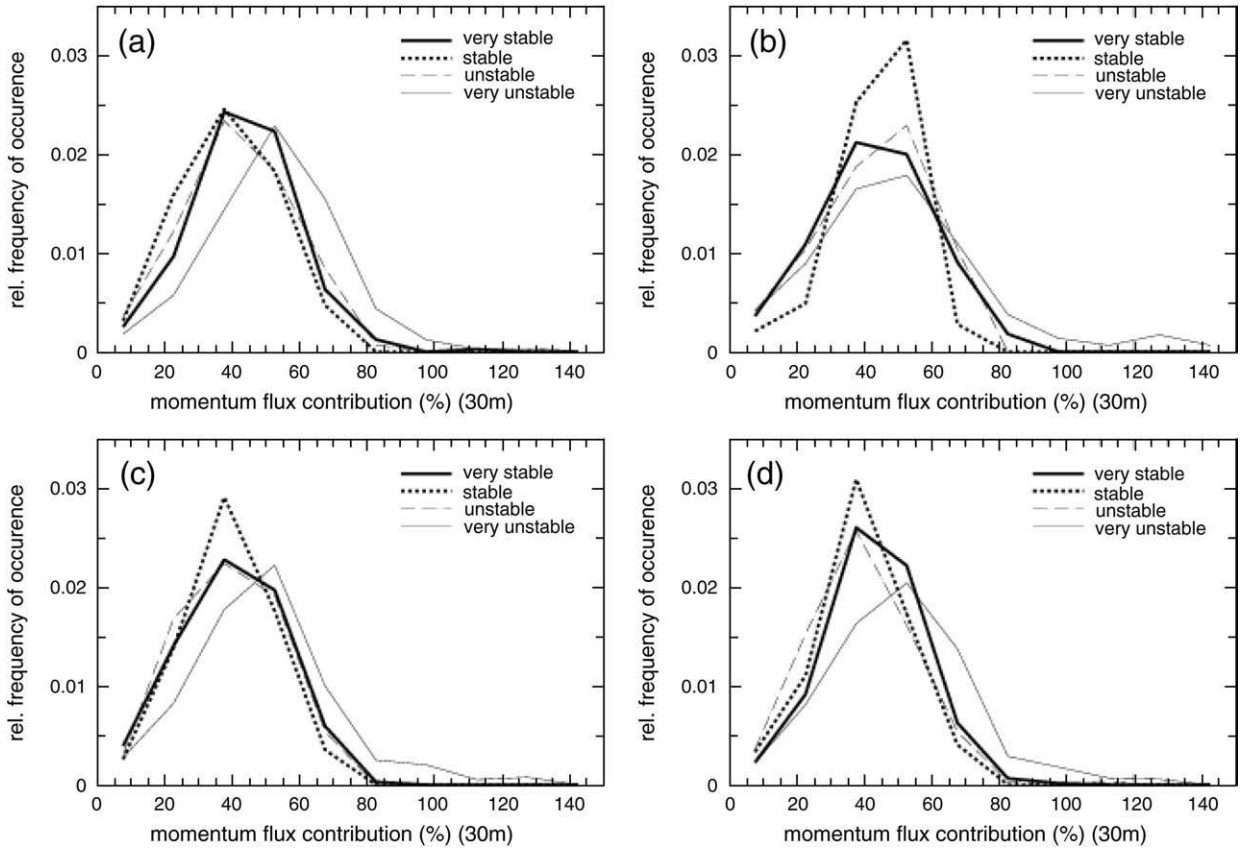

Fig. 8. Probability distribution functions of the contribution of the coherent structures to the total turbulent momentum fluxes, obtained from the measurements collected at 30 m as function of stratification. Panels a, b, c and d correspond to the north (close forest), east (distant forest), south (buildings) and west (open field) sectors, respectively.

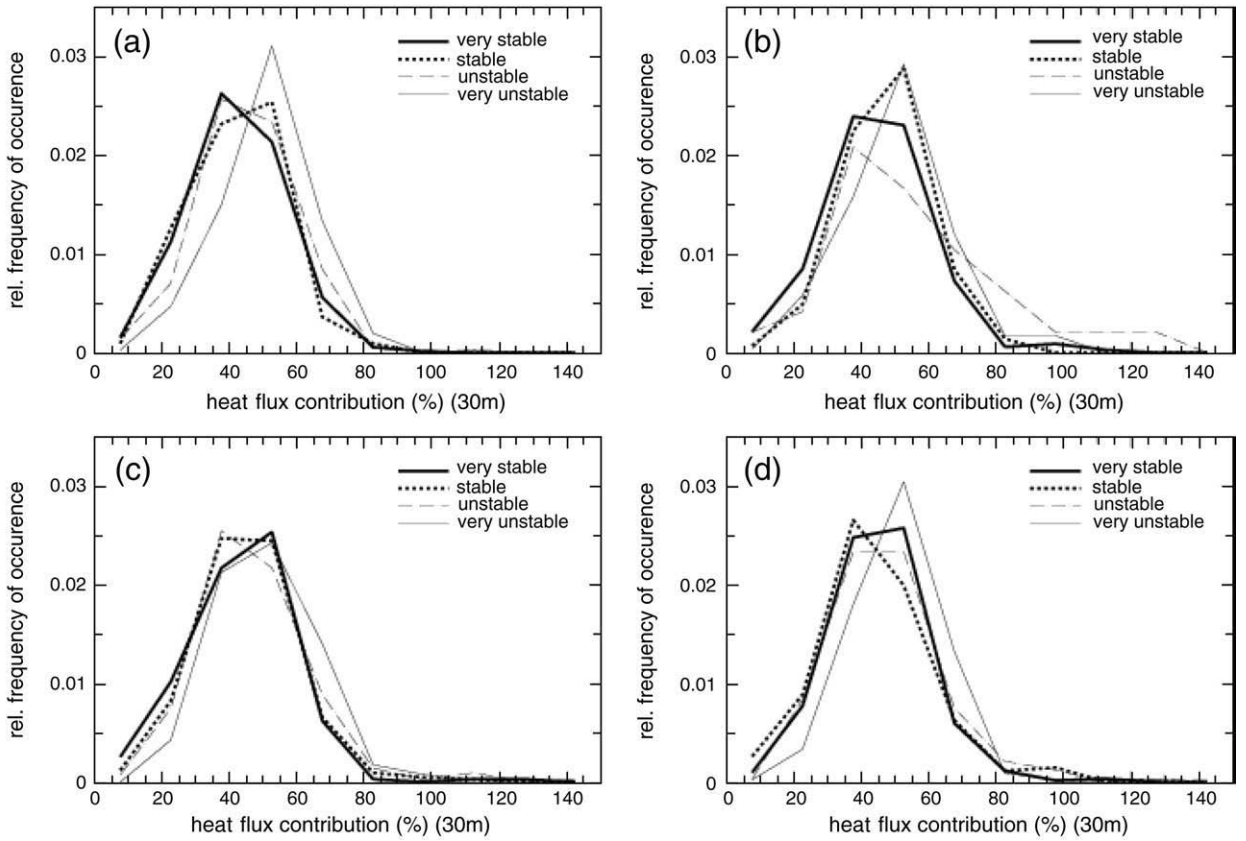

Fig. 9. Similar as Fig. 8 for heat flux.

which displays the PDF of the coherent structure contribution to the momentum fluxes and shows that whatever the upstream roughness, coherent structures are, on the average, not the dominant processes for the turbulent transport for most of the stability classes (Table 1), the meanvalues ranging between 31 and 57%.

A trend which seems to be verified for all wind sectors is that the contribution of the coherent structures to the momentum fluxes is more important in the very stable case. Fig. 9 shows the probability density functions of the coherent structures contribution to the heat flux. There again, the PDFs are very similar for all wind sectors (which is also expected because of the weak dependence of the average sensible heat flux to the upstream roughness, see Section 3) with a mean value of 46% (Table 2).

Table 3 shows the mean and dominant (most probable) values of the duration and separation times of the coherent structures detected at 30 m. It appears that, in average, the duration and separation times of the coherent structures increase with the instability. We notice no significant difference between 10 and 30 m measurement height. The mean duration time increases from about 60–70 s, in very stable and stable stratification, to about 80 and 100 s in unstable and very unstable PBL, respectively. This indicates that more unstable the PBL bigger the structures. However, the dominant duration of the coherent structures is about 50 s and does not vary significantly with the stability nor the wind sector. This observation is confirmed by Fig. 10 which represents the probability distribution functions of the duration time. Indeed, whatever the wind sector (panel a, b c or d), the distributions peaks are very close. However, in unstable condition, the distributions show more great values

Table 3
Mean and dominant (most probable) values of the duration (D) and separation (S) times for the four wind sectors and for the four stability classes.

	Very stable		Stable		Unstable		Very unstable	
	Mean	Dom.	Mean	Dom.	Mean	Dom.	Mean	Dom.
Close forest								
$D_{10\,m}$ (s)	64	50	60	40	82	60	90	60
$D_{30\,m}$ (s)	67	50	67	50	84	50	98	60
$S_{10\,m}$ (s)	79	15	82	15	101	15	96	15
$S_{30\,m}$ (s)	79	15	82	15	85	15	94	15
Distant forest								
$D_{10\,m}$ (s)	70	60	77	60	83	60	87	50
$D_{30\,m}$ (s)	68	60	66	50	85	70	96	50
$S_{10\,m}$ (s)	86	15	91	15	94	15	107	15
$S_{30\,m}$ (s)	87	15	83	15	108	15	126	15
Buildings								
$D_{10\,m}$ (s)	65	50	69	50	79	50	85	50
$D_{30\,m}$ (s)	67	50	68	50	82	60	99	60
$S_{10\,m}$ (s)	84	15	91	15	93	15	107	15
$S_{30\,m}$ (s)	86	15	96	15	100	15	120	15
Open field								
$D_{10\,m}$ (s)	64	50	64	50	88	40	89	60
$D_{30\,m}$ (s)	63	50	66	40	87	50	96	60
$S_{10\,m}$ (s)	82	15	81	15	109	15	103	15
$S_{30\,m}$ (s)	78	15	93	15	102	15	113	15

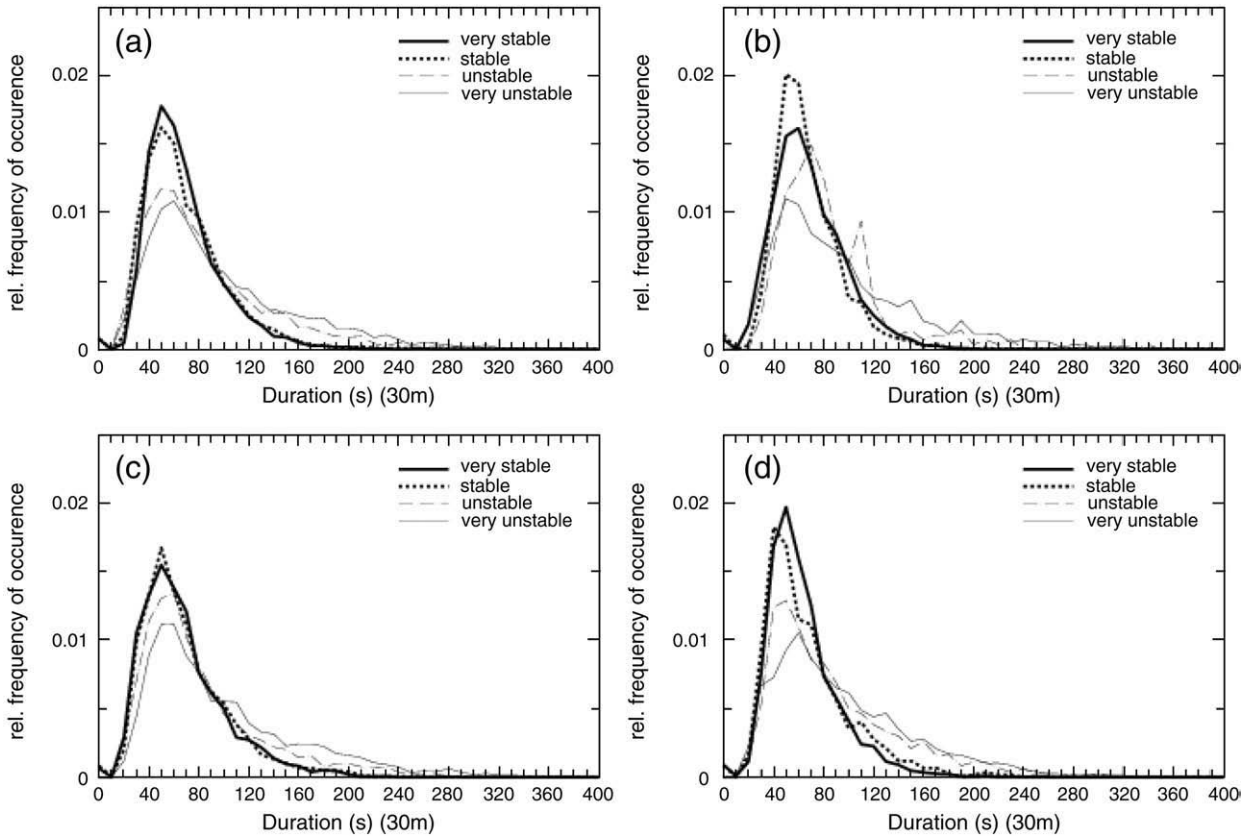

Fig. 10. Probability distribution functions of coherent structure duration at 30 m as function of stratification. Panels a, b, c and d correspond to the north (close forest), east (distant forest), south (buildings) and west (open field) sectors, respectively.

which explain the grater mean values in these stability classes. As regards the separation time, the mean value increase from about 80 to 90 s in stable and very stable conditions to about 100–120 s in unstable and very unstable conditions (Table 3). The probability distribution functions of the separation time are very similar, the wind sectors and the stability seem almost to have no influence on the time between two consecutive structures (Fig. 11). We can also notice that the dominant value is surprisingly exactly the same, 15 s (Table 3). This small value in comparison to the averaged one seems to indicate that we detect packets of coherent structures.

The independence of the coherent structure properties to the upstream roughness, in all stability conditions, is a key outcome of this study, considering that conversely, the average turbulence variables are strongly dependent on the upstream terrain complexity, whatever the stratification. This result extends the findings of Fesquet et al. (2008) and Fesquet et al. (in press) to the stable and unstable cases (including the very stable and very unstable PBLs). In these studies, LES simulations of neutral PBL including the effects of plant–atmosphere interactions were run to investigate the influence of surface inhomogeneities on near-surface coherent structures with configurations similar the north (close forest) and west (open field) sectors of our experimental site. The simulations of the neutral PBL were in excellent agreement with the observations collected in near-neutral stratification considering on the one hand the turbulent fluxes and kinetic energy, and on the other hand the coherent structure properties derived in the same way as in Barthlott et al. (2007) and in the present study: for the open field case, 7 to 14 structures were detected per 30 min in the LES, contributing to about 36 to 52% to the turbulent fluxes, whereas for the inhomogeneous terrain case, 9 to 14 structures were detected contributing to 39 to 55% to the turbulent fluxes.

In Fesquet et al. (2008) and Fesquet et al. (in press), the analysis of coherent structure trajectories, in neutral PBL, showed that structures are created significantly above the topographical elements (between $z = 50$ and 100 m). These structures can be produced through shear (e.g. Fesquet et al., 2008, in press; Drobinski and Foster, 2003; Drobinski et al., 2004) and/or convective (e.g. Drobinski et al., 1998) instability. Then, they seem transported downward onto the ground in agreement with recent observations of Drobinski et al. (2004), and confirming the 'top–down' behavior of coherent structures in the atmospheric surface layer as initially proposed by Hunt and Morrison (2000), Hunt and Carlotti (2001) and Carlotti (2002). As a result, the properties carried out by the large-scale outer eddies become independent from the nature of the terrain. Conversely, near-surface small-scale inner turbulence depends on the roughness elements since formed at the ground by convective instability

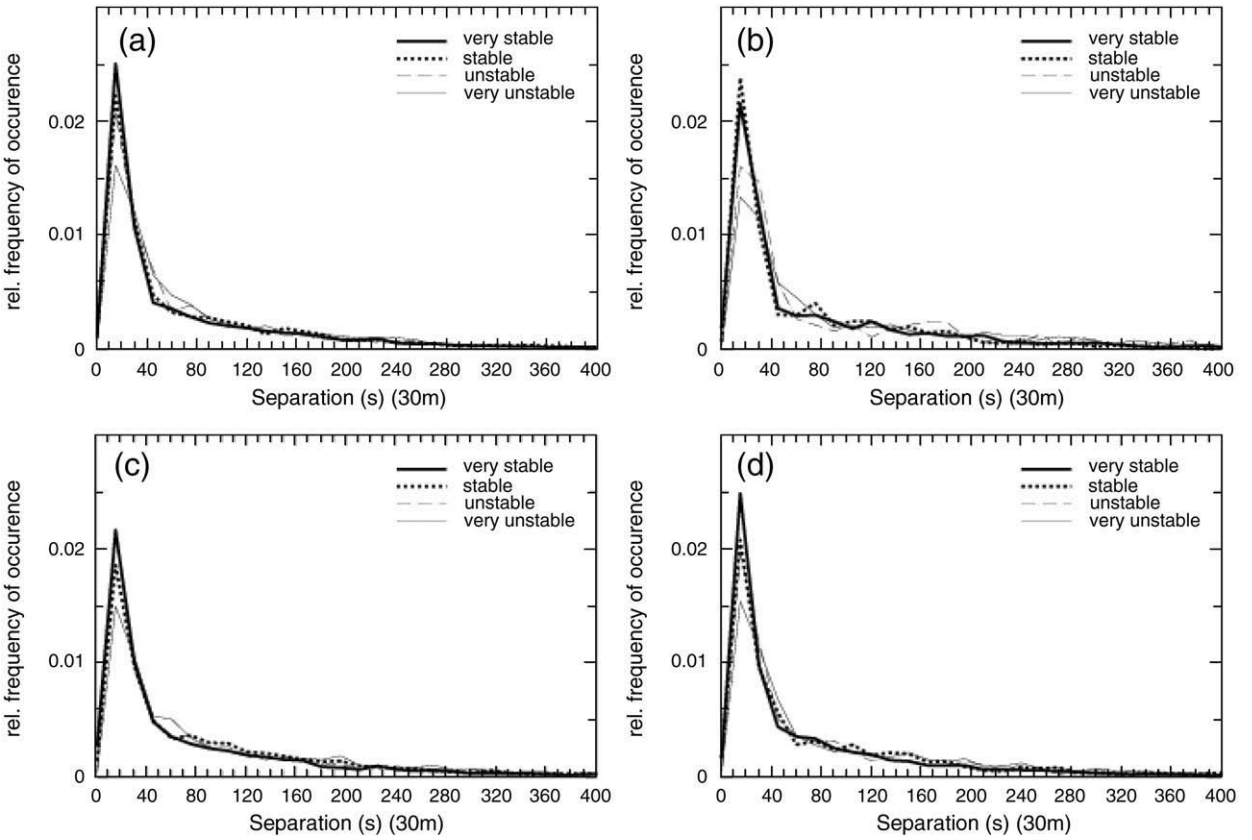

Fig. 11. Probability distribution functions of coherent structure separation at 30 m as function of stratification. Same labelling as Fig. 10.

(as suggested by McNaughton (2004)) or by shear and blocking at the surface (as suggested by Hunt and Morrison (2000)) where it can also interact with large-scale outer layer turbulence (McNaughton and Brunet, 2002).

Quantitatively, we can separate the coherent structure properties into two categories. On the one hand, the structural properties, i.e. the separation time between consecutive coherent structures, the coherent structure duration and the frequency of occurrence appear to be independent of the upstream condition in absolute value. This means that the presence of roughness elements does not contribute to the generation of more or less coherent structures and has no impact on the life time of these structures. Conversely, considering the energetic properties, only the contribution of coherent structures to the total surface fluxes does not depend on the terrain heterogeneity, but the surface fluxes associated to the coherent structures behave similarly as the average turbulent fluxes affected by upstream roughness. In other words, the intensity of near-surface turbulence and fluxes increases with upstream roughness (i.e. with increasing shear, see Barthlott et al. (2007), for stable stratification) but the contribution of the coherent structures to the fluxes remains unchanged whatever the terrain complexity.

5. Conclusion

This study investigates the impact of surface heterogeneity and stratification on local turbulence measurements using 18 months of turbulence measurements by sonic anemometers at 10 and 30 m heights on the 30 m tower of the SIRTA sub-urban observatory, under varying meteorological conditions and fetch configurations.

The data set extends the results of Fesquet et al. (2008, in press) from very stable to very unstable cases and this paper shows that no significant differences are found between the different stability class: the terrain complexity has an important impact on the various average turbulence variables like turbulent kinetic energy, and momentum fluxes whereas the upstream complexity of the terrain has no impact on the coherent structure properties, whatever the stability conditions. Indeed, the frequency of occurrence, the duration time of the coherent structures, the separation time between consecutive coherent structures and the relative contribution of the coherent structures to the total fluxes (momentum and heat) appear to be independent from the upstream roughness in all stability classes. The stability conditions have an impact on the structural properties of the coherent structures; more unstable, bigger than the coherent structures. So, in unstable regimes, we detect less structures but bigger ones.

This paper shows evidence of non-significant impact of the stability conditions on the turbulent processes in the presence of upstream heterogeneity and advocates for similar process for all stability conditions: large coherent structures (inactive turbulence in the Townsend sense) are created significantly above the canopy, in the outer layer, through shear and/or convective instability and are transported downward onto the

ground. When impinging onto the ground, they create an internal boundary layer where smaller structures (active turbulence) are created locally at the surface and carry properties independent of the surface heterogeneity.

These results are important since the coherent structures are known to be crucial in momentum, heat and mass transfers between the surface and the atmosphere. A better understanding of their 'universal' properties whatever the stability class should facilitate their parametrisation in meteorological models even in the presence of important heterogeneity. A further step of the current work could consist in performing a LES, in convective and stable, PBLs with other types of surface heterogeneities, representative of rural or urban canopies.

Acknowledgements

We would like to thank KG McNaughton for the fruitful discussions; M.C. Lanceau for their help in collecting the referenced papers. This research has been funded by the Centre National de la Recherche Scientifique (CNRS), the Direction Générale de l'Armement (DGA) and the Institut des Sciences de l'Univers (INSU) through the Programme Atmosphére Océan à Multi-échelle (PATOM). Christian Barthlott's visit at LMD was supported by the École Polytechnique. We are also grateful to the SIRTA scientific director M. Haef-felin, to the SIRTA project engineer C. Pietras and the SIRTA team. Wavelet software was provided by C. Torrence and G. Compo, and is available at URL: http://paos.colorado.edu/research/wavelets/.

References

Al-Jiboori, M.H., Y., X., Yongfu, Q., 2001. Turbulence characteristics over complex terrain in west China. Bound.-Lay. Meteorol. 101, 109–126.
Antonia, R.A., Chambers, A.J., Friehe, C.A., Van Atta, C.W., 1979. Temperature ramps in the atmospheric surface layer. J. Atmos. Sci. 36, 99–108.
Baldocchi, D.D., Hutchinson, B.A., 1987. Turbulence in an almond orchard: vertical variations in turbulent statistics. Bound.-Lay. Meteorol. 40, 127–146.
Baldocchi, D.D., Meyers, T.P., 1988. Turbulence structure in a deciduous forest. Bound.-Lay. Meteorol. 43, 345–364.
Barthlott, C., Fiedler, F., 2003. Turbulence structure in the wake region of a turbulent tower. Bound.-Lay. Meteorol. 108, 175–190.
Barthlott, C., Drobinski, P., Fesquet, C., Dubos, T., Pietras, C., 2007. Long-term study of coherent structures in the atmospheric surface layer. Bound.-Lay. Meteorol. 125 (1), 1–24 Oct.
Bradley, E.F., 1968. A micrometeorological study of velocity profiles and surface drag in the region modified by a change in surface roughness. Q. J. R. Meteorol. Soc. 116, 361–379.
Brunet, Y., Irvine, M.R., 2000. The control of coherent eddies in vegetation canopies: streamwise structure spacing, canopy shear scale and atmospheric stability. Bound.-Lay. Meteorol. 94, 139–163.
Businger, J.A., Wyngaard, J.C., Izumi, Y., Bradley, E.F., 1971. Flux profile relationships in the atmospheric surface layer. J. Appl. Meteorol. 28, 181–189.
Carlotti, P., 2002. Two-point properties of atmospheric turbulence very close to the ground: comparison of a high resolution les with theoretical models. Boundary-Lay. Meteorol. 104 (3), 381–410 Sep.
Champagne, F.H., Friehe, C.A., LaRue, J.C., Wyngaard, J.C., 1977. Flux measurements, flux estimation techniques, and fine-scale turbulence measurements in the unstable surface layer over land. J. Atmos. Sci. 34.
Chen, W., Novak, M.D., Black, T.A., Lee, X., 1997. Coherent eddies and temperature structure functions for three contrasting surfaces. Part I: Ramp model with finite microfront time. Bound.-Lay. Meteorol. 84, 99–123.
Claussen, M., 1987. The flow in a turbulent boundary layer upstream of a change in surface roughness. Bound.-Lay. Meteorol. 40, 31–86.
Collineau, S., Brunet, Y., 1993a. Detection of turbulent coherent motions in a forest canopy, Part 1: Wavelet analysis. Bound.-Lay. Meteorol. 65, 357–379.
Collineau, S., Brunet, Y., 1993b. Detection of turbulent coherent motions in a forest canopy, Part 2: Time-scales and conditional averages. Bound.-Lay. Meteorol. 66, 49–73.
Courault, D., Drobinski, P., Brunet, Y., Lacarrère, P., Talbot, C., 2007. Impact of surface heterogeneity on a buoyancy-driven convective boundary layer in light winds. Bound.-Lay. Meteorol. 124, 383–403.
Deardorff, J.W., 1972. Numerical investigation of neutral and unstable planetary boundary layers. J. Atmos. Sci. 29, 91–115.
Drobinski, P., Foster, R.C., 2003. On the origin of near-surface streaks in the neutrally stratified planetary boundary layer. Bound.-Lay. Meteorol. 108, 247–256.
Drobinski, P., Brown, R., Flamant, P., Pelon, J., 1998. Evidence of organised large eddies by ground-based doppler lidar, sonic anemometer and sodar. Bound.-Lay. Meteorol. 88, 343–361.
Drobinski, P., Carlotti, P., Newson, R.K., Banta, R.M., Foster, R.C., Redelsperger, J.L., 2004. The structure of the near-neutral atmospheric surface layer. J. Atmos. Sci. 61 (6), 699–714 Mar.
Drobinski, P., Foster, R.C., Pietras, C., 2006. Evaluation of a planetary boundary layer subgrid-scale model that accounts for near-surface turbulence anisotropy. Geophys. Res. Lett. 108, 247–256.
Drobinski, P., Carlotti, P., Redelsberger, J.-L., Banta, R.M., Masson, V., Newsom, R.K., 2007. Numerical and experimental investigation of the neutral atmospheric surface layer. J. Atmos. Sci. 64, 137–156.
Dyer, A.J., 1974. A review of flux-profile relationships. Bound.-Lay. Meteorol. 7, 363–372.
Etling, D., Brown, R.A., 1993. Roll vortices in the planetary boundary layer: a review. Bound.-Lay. Meteorol. 21, 215–248.
Feigenwinter, C., Vogt, R., 2005. Detection and analysis of coherent structures in urban turbulence. Theor. Appl. Climatol. 81, 219–230.
Fesquet, C., Dupont, S., Drobinski, P., Barthlott, C., Dubos, T., 2008. Impact of terrain heterogeneities on coherent structures properties: experimental and numerical approaches. 18th Symposium on Boundary Layers and Turbulence. No. 11B.1. Stockholm, Sweden.
Fesquet, C., Dupont, S., Drobinski, P., Dubos, T., Barthlott, C., in press. Impact of terrain heterogeneity on coherent structure properties: numerical approach. Bound.-Layer Meteorol.
Foster, R.C., Brown, R.A., 1994. On large-scale PBL modelling: Surface layer models. The Global Atmosphere and Ocean System 2, 185–198.
Gao, W., Li, B.L., 1993. Wavelet analysis of coherent structures at the atmosphere–forest interface. J. Appl. Meteorol. 32, 1717–1725.
Gao, W., Shaw, R.H., Paw, U.K.T., 1989. Observation of organized structure in turbulent flow within and above a forest canopy. Bound.-Lay. Meteorol. 47, 349–377.
Gao, W., Shaw, R.H., Paw, U.K.T., 1992. Conditional analysis of temperature and humidity microfronts and ejection/sweep motions within and above a deciduous forest. Bound.-Lay. Meteorol. 59, 35–57.
Garratt, J.R., 1990. The internal boundary layer — a review. Bound.-Lay. Meteorol. 50, 171–203.
Gash, J.H.C., 1986. Observations of turbulence downwind of a forest–heath transition. Bound.-Lay. Meteorol. 36, 227–237.
Haeffelin, M., Barthès, L., Bock, O., Boitel, C., Bony, S., Bouniol, D., Chepfer, H., Chiriaco, M., Delanoë, J., Drobinski, P., Dufresne, J., Flamant, C., Grall, M., Hodzic, A., Hourdin, F., Lapouge, F., Lemaître, Y., Mathieu, A., Morille, Y., Naud, C., Noël, V., Pelon, J., Pietras, C., Protat, A., Romand, B., Scialom, G., Vautard, R., 2005. Sirta, a ground-based atmospheric observatory for cloud and aerosol research. Ann. Geophys. 23, 253–275.
Hunt, J.C.R., Carlotti, P., 2001. Statistical structure at the wall of the high Reynolds number turbulent boundary layer. Flow Turbulence And Combustion 66 (4), 453–475.
Hunt, J.C.R., Morrison, J.F., 2000. Eddy structure in turbulent boundary layers. Eur. J. Mech. B/Fluids 19, 673–694.
Irvine, M.R., Gardiner, B.A., Fiedler, F., 1997. The evolution of turbulence across a forest edge. Bound.-Lay. Meteorol. 84, 467–496.
Karlsson, S., 1986. The applicability of wind profile formulas to an urban–rural interface site. Bound.-Lay. Meteorol. 34, 333–355.
Kastner-Klein, P., Rotach, M.W., 2004. Mean flow and turbulence characteristics in an urban roughness sublayer. Bound.-Lay. Meteorol. 111, 55–84.
Kruijt, B., Malhi, Y., Lloyd, J., Nobre, A.D., Miranda, A.C., Pereira, M.G.P., Culf, A., Grace, J., 2000. Turbulence statistics above and within two Amazon rain forests canopies. Bound.-Lay. Meteorol. 94, 297–331.
Krusche, N., De Oliveira, A.P., 2004. Characterization of coherent structures in the atmospheric surface layer. Bound.-Lay. Meteorol. 110, 191–211.
Lien, F.S., Yee, E., 2004. Numerical modelling of the turbulent flow developing within and over a 3-D building array, part I: a high-resolution Reynolds-averaged Navier–stokes approach. Bound.-Lay. Meteorol. 112, 427–466.
Liu, J., Chen, J.M., Black, T.A., Novak, M.D., 1996. E–ε modelling of turbulent air flow downwind of a model forest edge. Bound.-Lay. Meteorol. 77 (1), 21–44 Jan.
Lu, C.-H., Fitzjarrald, D.R., 1994. Seasonal and diurnal variations of coherent structures over a deciduous forest. Bound.-Lay. Meteorol. 69, 43–69.

Mahrt, L., 1996. The bulk aerodynamic formulation over heterogeneous surfaces. Bound.-Lay. Meteorol. 78, 87–119.
Mahrt, L., 1999. Stratified atmospheric boundary layers. Bound.-Lay. Meteorol. 90, 375–396.
Marcolla, B., Pitacco, A., Cescatti, A., 2003. Canopy architecture and turbulence structure in a coniferous forest. Bound.-Lay. Meteorol. 108, 39–59.
McAneny, K., Baille, A., Sappe, G., 1988. Turbulence measurements during mistral winds with a 1-dimensional sonic anemometer. Bound.-Lay. Meteorol. 42.
McNaughton, K.G., 2004. Attached eddies and production spectra in the atmospheric logarithmic layer. Bound.-Lay. Meteorol. 111, 1–18.
McNaughton, K.G., Brunet, Y., 2002. Townsend's hypothesis, coherent structures and Monin–Obukhov similarity. Bound.-Lay. Meteorol. 102 (2), 161–175.
Monin, A.S., Obukhov, A.M., 1954. Basic laws of turbulent mixing in the ground layer of the atmosphere. Trans. Geophys. Inst. Akad. Nauk. USSR 151, 163–187.
Morrison, I., Businger, S., Marks, F., Dodge, P., Businger, J., 2005. An observational case for the prevalence of roll vortices in the hurricane boundary layer. J. Atmos. Sci. 62, 2662–2673.
Morse, A.P., Gardiner, B.A., Marshall, B.J., 2002. Mechanisms controlling turbulence development across a forest edge. Bound.-Lay. Meteorol. 103, 227–251.
Nord, M., 1991. Shelter effects of vegetation belts — results of field measurements. Bound.-Lay. Meteorol. 54, 363–385.
Patton, E.G., Sullivan, P.P., Moeng, C.-H., 2005. The influence of idealized heterogeneity on wet and dry planetary boundary layers coupled to the land surface. J. Atmos. Sci. 62, 2078–2097.
Peters, G., Fischer, B., Kirtzel, H.J., 1998. One-year operational measurements with a sonic anemometer–thermometer and a doppler sodar. J. Atmos. Oceanic Technol. 15.
Qiu, J., Paw, U.K.T., Shaw, R.H., 1995. Pseudo-wavelet analysis of turbulence patterns in three vegetation layers. Bound.-Lay. Meteorol. 72, 177–204.
Raine, J.K., Stevenson, D.C., 1977. Wind protection by model fences in a simulated atmospheric boundary layer. J. Indust. Aero. 2, 159–180.
Raupach, M.R., Coppin, P.A., Legg, B.J., 1986. Experiments on scalar dispersion within a model plant canopy. Part I: the turbulent structure. Bound.-Lay. Meteorol. 35, 21–52.
Raynor, G.S., 1971. Wind and temperature structure in a coniferous forest and a contiguous field. For. Sci. 17, 351–363.
Seginer, I., Mulhearn, P.J., Bradley, E.F., Finningan, J.J., 1976. Turbulent flow in a model plant canopy. Bound.-Lay. Meteorol. 10, 423–453.
Stull, R., 1988. An introduction to boundary layer meteorology. Kluwer Academic Publishers, Dordrecht. 666 pp.
Taylor, P.A., 1968. The planetary boundary layer above a change in surface roughness. J. Atmos. Sci. 26, 432–440.
Torrence, C., Compo, G.P., 1998. A practical guide to wavelet analysis. Bull. Amer. Meteor. Soc. 79, 61–78.
Vickers, D., Mahrt, L., 1997. Quality control and flux sampling problems for tower and aircraft data. J. Atmos. Ocean. Technol. 14, 512–526.
Villani, M.G., 2003. Turbulence statistics measurements in a northern hardwood forest. J. Atmos. Sci. 108, 343–364.